

Journal of Materials Chemistry A

Accepted Manuscript



This is an *Accepted Manuscript*, which has been through the Royal Society of Chemistry peer review process and has been accepted for publication.

Accepted Manuscripts are published online shortly after acceptance, before technical editing, formatting and proof reading. Using this free service, authors can make their results available to the community, in citable form, before we publish the edited article. We will replace this *Accepted Manuscript* with the edited and formatted *Advance Article* as soon as it is available.

You can find more information about *Accepted Manuscripts* in the [Information for Authors](#).

Please note that technical editing may introduce minor changes to the text and/or graphics, which may alter content. The journal's standard [Terms & Conditions](#) and the [Ethical guidelines](#) still apply. In no event shall the Royal Society of Chemistry be held responsible for any errors or omissions in this *Accepted Manuscript* or any consequences arising from the use of any information it contains.

Cocatalyst-Free CdS nanorods/ZnS nanoparticles Composite for High-Performance Visible-Light-Driven Hydrogen Production from Water

Daochuan Jiang, Zijun Sun, Hongxing Jia, Dapeng Lu, Pingwu Du*

Key Laboratory of Materials for Energy Conversion, Chinese Academy of Sciences, Department of Materials Science and Engineering, *iChEM* (Collaborative Innovation Center of Chemistry for Energy Materials), University of Science and Technology of China, Hefei, Anhui Province, 230026, P. R. China

*To whom correspondence should be addressed

E-mail: dupingwu@ustc.edu.cn

Tel/Fax: 86-551-63606207

Abstract: Highly efficient, visible-light-induced hydrogen (H_2) production *via* water splitting can be achieved without the help of a cocatalyst by a noble-metal-free core-shell photocatalyst, in which zinc sulfide (ZnS) nanoparticles as the protective shell is anchored on the surface of cadmium sulfide nanorods (CdS NRs). Due to the closely interfacial contact of component semiconductors, the electronic structure of CdS is strongly coupled with that of ZnS nanoparticles, leading to an efficient transfer of charge carriers between them and the improvement of the CdS photostability. The CdS/ZnS NRs photocatalyst showed much higher catalytic activity for H_2 production than CdS NRs and ZnS under visible light irradiation ($\lambda > 420$ nm), which is probably due to fast transfer of the photogenerated charge carriers and/or electron tunneling in one-dimensional core-shell nanorod structure. Under optimal conditions, the highest hydrogen evolution rate reached $239 \mu\text{mol}\cdot\text{h}^{-1}\cdot\text{mg}^{-1}$, which is much greater than ZnS and CdS NRs and also among the best cocatalyst-free photocatalysts for H_2 production. The average apparent quantum yield can be achieved as $\sim 16.8\%$ after 8 h of irradiation (monochromatic light at $420 \text{ nm} \pm 5 \text{ nm}$). A possible mechanism for the photocatalytic reaction based on CdS/ZnS NRs is also discussed.

Keywords: Cocatalyst-free; Hydrogen production; Photocatalysis; Core-shell structure; Nanorod

Introduction

Development of clean and renewable energy has been one of a hot subject in recent decades as a result of the global energy crisis. One way to address this issue is the use of solar energy over semiconductor photocatalysts¹⁻² or molecular catalysts³⁻⁷ for hydrogen (H₂) production. Extensive efforts have been focused on finding the suitable semiconductors for this purpose, including efforts with metal oxides,⁸⁻¹¹ metal hydroxides,¹²⁻¹³ oxynitrides,¹⁴⁻¹⁷ sulfides,¹⁸⁻¹⁹ and metal-free semiconductors.²⁰⁻²¹ However, the most widely studied semiconductors, such as TiO₂ and ZnO, mainly absorb the ultraviolet photons that account for less than 5% of solar light.²² Therefore, seeking a robust semiconductor photocatalyst which can efficiently utilize visible light is an important topic in this area.

CdS is a very promising n-type semiconductor for photocatalytic H₂ production due to its low band gap energy (~2.4 eV) and high activity under visible light.²³⁻²⁴ However, CdS suffers from severe photocorrosion and fast recombination of photogenerated charge carriers under visible light.²⁵⁻²⁷ To overcome these drawbacks, various cocatalysts have been studied to functionalize CdS nanoparticles to improve the catalytic activity,²⁸ in which the cocatalysts could accept photoinduced electrons and retard the charge recombination process (Scheme 1a). These cocatalysts include both noble-metal-based materials (Pt, Pd, Ru, etc)^{25,29-30} and noble-metal-free materials (Ni, Co, Cu, etc).^{6-7,31-32} In addition, dual cocatalysts can highly enhance the quantum efficiency (up to ~93%) for photocatalytic H₂ production in water (for example, the Pt-PdS/CdS system) (Scheme 1b).²⁵ Different morphologies of CdS

semiconductor were also explored for photocatalysis (Scheme 1c only show the nanorod morphology; many others, such as nanosheet and nanocube, are not shown).³³⁻³⁵ Another strategy is to couple CdS with other semiconductors with suitable bandgaps to facilitate charge transfer and separation (Scheme 1d). A few examples have been reported in the literature for photocatalytic H₂ production.³⁶⁻³⁷ The typical semiconductor composites used for this purpose include nanoparticulate CdS/TiO₂,^{19,36,38} CdS/Cu₂O,³⁹ and CdS/ZnO.⁴⁰⁻⁴¹ ZnS material has also demonstrated to promote the catalytic activities due to the appropriate structural arrangement/morphology of the photocatalyst,⁴²⁻⁴⁴ in which the trap states in the CdS core materials can be reduced by ZnS layer. However, the catalytic performance of such a heterostructured photocatalyst is still quit low. The nature of electron transport in nanoparticulate materials is fairly well studied.⁴⁵⁻⁴⁶ Time-resolved measurements⁴⁵⁻⁴⁷ and modelling studies⁴⁸⁻⁴⁹ indicate that electron transport in nanoparticles proceeds by a trap-limited diffusion process but the diffusion length is limited by the size of particles and crystallinity. It has been reported that single-crystalline nanowires/nanorods can increase the electron diffusion length, which could be several orders of magnitude faster than that in a random polycrystalline nanoparticles.⁵⁰⁻⁵¹

Inspired by previous studies, to enhance the electron diffusion length in photocatalysis and improve the photocatalytic activity, herein we report the use of core-shell CdS nanorods/ZnS nanoparticles composite (CdS/ZnS NRs, Scheme 1e) as a very efficient photocatalyst without a cocatalyst for visible light-driven hydrogen

production from water with a H₂ evolution rate at $\sim 239 \mu\text{mol}\cdot\text{h}^{-1}\cdot\text{mg}^{-1}$. The nanorod samples were synthesized via a simple solvothermal step followed by a solution bath deposition method. Their physical properties were well characterized by scanning electron microscope (SEM), powder X-ray diffraction (XRD), transmission electron microscopy (TEM), high-resolution transmission electron microscopy (HRTEM), UV-vis diffuse reflectance spectroscopy (UV-vis DRS), and X-ray photoelectron spectroscopy (XPS). The photocatalytic reaction mechanism was proposed based on the photocurrent measurement.

Results and Discussion

Figure 1a shows the XRD patterns of pure CdS and core-shell CdS/ZnS photocatalysts with different mole ratios of ZnS. All the samples have similar diffraction peaks, which can be indexed to the hexagonal phase of CdS with crystalline parameters at $a = 4.141 \text{ \AA}$ and $c = 6.72 \text{ \AA}$. The peaks at 2θ of 24.81° , 26.51° , 28.18° , 36.62° , 43.68° , 47.84° , and 51.82° are assigned to diffraction patterns from the (100), (002), (101), (102), (110), (103), and (112) lattice planes of CdS (JCPDS 41-1049), respectively, indicating that crystalline CdS materials were successfully synthesized (Figure 1a).³³ It should be noted that strong CdS crystalline phases appeared in all these samples and no obvious diffraction peaks of ZnS were observed, probably because the amount of ZnS is too small and/or there was weak crystallization. For comparison, the XRD patterns of pure ZnS prepared by the same method can be indexed to cubic phase (JCPDS 05-0566), as shown in Figure 1b. The

weak crystallization of pure ZnS agrees well with the missing obvious ZnS diffraction peaks in the XRD patterns of core-shell CdS/ZnS materials. When the ratio of ZnS was further increased, the diffraction peaks can be found, as in the CdS/ZnS-5 sample (Figure 1a and Figure 1c). Based on above results, the presence of ZnS did not affect the crystallinity of CdS, indicating that ZnS did not dope into the crystal lattice of CdS.

The morphology of the samples was investigated by SEM and TEM. Figure 2a is the SEM image of pure CdS, demonstrating the nanorod morphology with a diameter of 30~60 nm and a length of 0.5~2 μm . When loading ZnS semiconductor nanoparticles onto CdS, the nanorod morphology of the material has no significant change, as shown in the CdS/ZnS-0.5 sample (Figure 2b). However, the nanorod surfaces became rough after the growth of ZnS nanoparticles, indicating the successful deposition of ZnS. The EDX spectrum of the sample shows the presence of Cd, S, Zn, Cu, and C elements (Figure 2b, inset). The Cu element is from the Cu grid substrate. In addition, TEM images confirmed the results observed in the SEM images. The TEM image of pure CdS showed similar nanorod morphology with smooth surfaces (Figure 2c). Compared with pure CdS, the formation of CdS/ZnS core/shell nanostructure was clearly observed for the ZnS/CdS NRs and the surfaces of the nanorods became rough with small nanoparticles (2-5 nm) on CdS NRs (Figure 2d and Figure S1). More importantly, the diameter of the CdS/ZnS NRs was increased ca. 2~6 nm when ZnS was deposited on the surface of CdS.

The core/shell structure of CdS/ZnS can be confirmed by elemental mapping.

The elements of Cd, Zn, and S were present, as shown in Figure 3a-3e. The distribution of each element and the difference in the width further indicate the ZnS shell was coated on the surfaces of the CdS NRs. Furthermore, the HRTEM image of the CdS/ZnS-0.5 sample showed a lattice fringe distance of 0.312 nm in the shell and 0.336 nm in the core, which can be assigned to the (111) plane of cubic ZnS and the (002) plane of hexagonal CdS, respectively (Figure 3f and Figure S2).

To identify the surface chemical composition and valence state of the core-shell semiconductor heterostructure, the XPS spectra of the CdS/ZnS-0.5 sample was measured. The XPS survey scan in Figure 4a shows the presence of Cd, S, Zn, and C elements. The C element at 285.2 eV was the reference to correct the binding energies. The high resolution XPS spectrum of Cd 3d shows two peaks at 404.49 eV and 411.23 eV, which are assigned to Cd 3d_{5/2} and Cd 3d_{3/2} in CdS,^{26-27,34} respectively (Figure 4b). The high resolution Zn 2p binding energies locate at around 1044.23 eV and 1021.21 eV, corresponding to Zn 2p_{1/2} and Zn 2p_{3/2}, respectively (Figure 4c).⁵²⁻⁵³ The high resolution XPS data of S exhibits two peaks (Figure 4d), the binding energies of S 2p_{3/2} and S 2p_{1/2} are 161.6 eV and 162.9 eV, respectively, which demonstrates the existence of S²⁻. All the binding energies indicate the formation of ZnS and CdS.

Photocatalytic hydrogen production experiments were carried out using the as-prepared photocatalysts in water under visible light irradiation ($\lambda > 420$ nm). Figure 5a shows the rate of H₂ evolution using CdS/ZnS samples with different amounts of ZnS in the presence of Na₂S and Na₂SO₃ as sacrificial reagents. It was

found that the rate of H₂ evolution initially increases and then decreases with an increasing amount of ZnS. The corresponding H₂ evolution rates are 195 $\mu\text{mol}\cdot\text{h}^{-1}\cdot\text{mg}^{-1}$, 239 $\mu\text{mol}\cdot\text{h}^{-1}\cdot\text{mg}^{-1}$, 150 $\mu\text{mol}\cdot\text{h}^{-1}\cdot\text{mg}^{-1}$, 118 $\mu\text{mol}\cdot\text{h}^{-1}\cdot\text{mg}^{-1}$, 68 $\mu\text{mol}\cdot\text{h}^{-1}\cdot\text{mg}^{-1}$, for the samples CdS/ZnS-0.1, CdS/ZnS-0.5, CdS/ZnS-1.0, CdS/ZnS-1.5, CdS/ZnS-5.0, respectively. The maximum rate of H₂ production was observed for CdS/ZnS-0.5. A corresponding animation of the H₂ production is shown in supporting information movie S1, with a large amount of H₂ bubbles produced from the solution. The present CdS/ZnS system has much higher H₂ production rate than other photocatalysts without loading a cocatalyst for H₂ production reported in the literature, such as CdS/TiO₂,³⁶ ZnO/ZnS,⁵⁴ NiS/CdS,³⁵ and Co₃O₄-CdS.³⁴ This result indicates that the CdS/ZnS-0.5 NRs have an optimal deposition amount, which favors the transport and separation of photogenerated charge carriers. A further increase in the amount of ZnS results in a decrease of the rate for photocatalytic H₂ production, which is possibly due to the decreased catalytic sites for H₂ evolution on the CdS surface when coated by more ZnS particles. Similar observations have also been previously reported.^{26,54} To further confirm the critical roles of the ZnS shell in the photocatalytic experiments, ZnS and CdS samples were used for comparison under the same condition. No appreciable hydrogen can be detected when ZnS alone was used as the catalyst, suggesting that pure ZnS is not active for photocatalytic H₂ production under the same conditions. The corresponding H₂ evolution rate of CdS was much less than that of CdS/ZnS-0.5. All of the above results indicate that ZnS can be used as an efficient promoter for photocatalytic H₂ production and plays an

important role in inhibition of the recombination of photogenerated electron-hole pairs. In addition, the photocatalytic activity for hydrogen production can be further enhanced by loading 1.0 wt% Pt (Figure S5a). The hydrogen evolution rate of $340 \mu\text{mol}\cdot\text{h}^{-1}\cdot\text{mg}^{-1}$ has been achieved because Pt is a well-known active cocatalyst for hydrogen production.

Determination of the apparent quantum yield (AQY) of the photocatalytic H_2 production was performed in a system containing 1.05 M Na_2SO_3 and 0.75 M Na_2S in 20 mL millipore water. Monochromatic light at 420 nm (± 5 nm) was used as the light source. The experiment was run for 8 h and the result is shown in Figure 5b. In the first hour, the AQY was 11.3%. After that, a slight increase to $\sim 18\%$ was obtained in the second hour and then remained relative stable in the following hours. The average AQY was calculated to be $\sim 16.8\%$ during 8 hours of irradiation. We also check the AQY for CdS/ZnS photocatalyst loaded with 1.0 wt% Pt (Figure S5b). As expected, the corresponding average AQY reached 22.8% after 6 hours of irradiation, which is higher than a Pt-free CdS/ZnS sample. This trend is consistent with the result shown in Figure S5a.

The stability of the CdS/ZnS-0.5 sample in terms of photocatalytic activity under visible light irradiation was further investigated. The reaction system was evacuated to remove the evolved H_2 inside the reaction flask every 3 h and the process was carried out for repeated cycles. As shown in Figure 5c, the ZnS/CdS-0.5 photocatalyst exhibited similar photocatalytic activity for 12 h, suggesting excellent stability of this material for H_2 production.

Furthermore, the long-term stability of the CdS/ZnS-0.5 for H₂ production was investigated. During the course of the experiment, the H₂ production rate was basically the same and 14 mmol H₂ was produced after 46 h of irradiation (Figure 5d). This result suggests that the CdS/ZnS-0.5 sample is a highly efficient photocatalyst with great stability under visible light irradiation in the present system. After photocatalysis, the morphology of the photocatalyst remained nearly the same (Figure S3) and powder XRD data is almost consistent with the sample before photocatalysis (Figure S4), confirming good stability of the present photocatalyst.

Figure 6a shows the influence of concentration of the sacrificial agents on H₂ production using CdS/ZnS NRs photocatalyst. The results show that the photocatalytic activity rapidly increased with increasing concentration of the Na₂S and Na₂SO₃. The reaction reached a maximum rate for H₂ evolution in the presence of 1.0 M Na₂S and 1.4 M Na₂SO₃. A further increase of the concentration resulted in a slightly reduced rate of H₂ production, probably due to the fact that loss of light energy results from the undissolved sacrificial agent in the oversaturated system.

The UV-vis diffuse reflectance absorption spectra of the CdS, ZnS, and CdS/ZnS-0.5 samples are shown in Figure 6b. Pure CdS can absorb visible light with a bandgap of ca. 2.39 eV (520 nm) and the absorption spectra of pure ZnS shows its wide band gap at ca. 3.38 eV (367 nm). It is observed that the absorption edge of the ZnS/CdS heterostructure shows a slight blueshift in the visible region compared with that of CdS, revealing a band gap broadening due to the wide band gap of ZnS.⁵⁵ This could be attributed to the interfacial interaction between ZnS and CdS.

Transient photocurrent response curves of the electrodes coated with CdS NRs and CdS/ZnS-0.5 samples were measured in an electrochemical potentiostat under visible light irradiation ($\lambda > 420$ nm) (Figure 7). The results show that the photocatalysts present very low dark current ($< 10^{-7}$ mA/cm²). However, when the visible light irradiation is turned on, the photocurrent rapidly increases to a constant value for both samples. Specifically, the CdS/ZnS-0.5 electrode exhibits a much higher photocurrent than that of pure CdS electrode, indicating the ZnS protective nanoparticles in CdS/ZnS-0.5 sample can efficiently facilitate the transport of photoinduced charge carriers under visible light irradiation.^{Zhang, 2015 #56} It would effectively prevent direct recombination of electrons and holes, allowing more electrons to be captured by protons to produce H₂. The faster charge carriers transfer process in CdS/ZnS sample can be further confirmed by time-resolved photoluminescence (TRPL) decay spectra (Figure S6). The results show that the lifetime of the excited states in CdS/ZnS sample is much shorter than that for pure CdS NRs, indicating the transfer of photoexcited charge carriers between CdS and ZnS probably exists. A similar observation can be found in the previous literature.⁴³

It has been established that the bandgap of ZnS is much wider than that of CdS, and ZnS has both a higher conduction band (CB) and deeper valence band (VB).^{19,56} Typically, the transfer of the photogenerated electrons and holes will be limited in a well-confined type-I structure. From this point of view, the CdS/ZnS catalyst should not be more active for hydrogen evolution than pure CdS. However, our present study and other reported results^{43-44,57} do indicate efficient transfer of charge carriers in the

core-shell CdS/ZnS system. The phenomena can be achieved through two possible mechanisms: a hole transfer mechanism and an electron tunneling mechanism (Scheme 2). As drawn in Scheme 2A, there are many intrinsic defects, such as zinc vacancies (V_{Zn}) and interstitial sulfur vacancies (I_s) in the ZnS shells. V_{Zn} and I_s can act as acceptors for holes generated in the CdS NRs, which further promotes efficient charge transfer, thereby stimulating efficient H_2 production. Thus, a tentative mechanism for the enhanced photocatalytic activity of the CdS/ZnS sample is proposed and the CB/VB levels of the CdS and ZnS are illustrated according to previous reports.^{56,58} Under visible light illumination, the electrons located on the valence band (VB) of CdS are excited to the conduction band (CB), accompanied by the creation of holes in the VB. When ZnS shell is introduced onto the photocatalyst, holes from CdS Fermi level are splitted into the ZnS hole Fermi level and a more efficient hole transfer process from CdS to ZnS can occur.⁵⁷ The spatial separation of photogenerated electrons and holes is probably responsible for the enhanced photocatalytic activity for H_2 production in our CdS/ZnS NRs system. This is indicated by the higher photocurrent responses for CdS/ZnS-0.5 in Figure 7. On the other hand, taking the ZnS shell thickness (< 10 nm) into account, there may exist another possible electron tunneling pathway for electron transfer (Scheme 2B), which was recognized in the type I core/shell nanocrystals (NCs), such as CdSe/CdS core/shell NCs,⁵⁹ and CdS/ZnS core/shell NCs.³¹ In this case, the surface-deep trap states of CdS core, on which the photogenerated electrons and holes with low energy are not efficient for hydrogen evolution, is passivated, making more charge carriers

with suitable energies active for reduction reaction. Thus, the charge carriers in the CdS core might tunnel through thin ZnS shell for photocatalytic hydrogen evolution. In addition, the charge carriers may also leak from the uncovered CdS nanorod surface to outside. Therefore, the above-mentioned pathways are probably responsible for the enhanced photocatalytic hydrogen production.

Conclusions

In summary, CdS/ZnS core/shell NRs photocatalyst was successfully synthesized by a facile method. The photocatalytic activity can be significantly enhanced by addition of a ZnS shell. The ZnS/CdS-0.5 sample exhibited a maximum H₂ production of $\sim 239 \mu\text{mol}\cdot\text{h}^{-1}\cdot\text{mg}^{-1}$. The apparent quantum yield was $\sim 16.8\%$ after 8 hours of irradiation under optimal conditions. The results indicate that ZnS can efficiently facilitate the spatial separation of photogenerated charge carriers and highly promote photocatalytic activity for H₂ evolution. This work provides a novel noble-metal-free core-shell CdS/ZnS system without a cocatalyst for highly efficient photocatalytic H₂ evolution with good stability in water.

Experimental Details

Synthesis of the photocatalysts. All chemicals were commercially available and used without further purification. Pure CdS NRs were prepared by a modified one-step solvothermal method.⁶⁰ In a typical procedure, 4.62 g of CdCl₂·2.5H₂O and 4.62 g of CH₄N₂S were dissolved in 60 ml of ethylenediamine. The mixture was

transferred into a Teflon-lined autoclave, sealed, and maintained at 160 °C for more than 48 h. After cooling to room temperature, the resulting yellow solid products were collected by centrifugation, washed with distilled water and ethanol three times each. The product was then dried at 60 °C overnight. ZnS shells were coated on the surface of CdS NRs based on chemical bath deposition reaction using $\text{Zn}(\text{NO}_3)_2 \cdot 6\text{H}_2\text{O}$, citric acid, and Na_2S . Typically, 101 mg (0.7 mmol) CdS NRs and 20 mg (0.095 mmol) citric acid were added into 50 mL distilled water. The mixture was ultrasonicated for 10 min and then maintained at 40 °C for 2 h with stirring. After cooling to room temperature, 20 mL aqueous solution of a certain amount of $\text{Zn}(\text{NO}_3)_2 \cdot 6\text{H}_2\text{O}$ was slowly added into the above reaction solution, followed by stirring for another hour. Next, 20 mL Na_2S aqueous solution (the molar ratio of $\text{Zn}(\text{NO}_3)_2 \cdot 6\text{H}_2\text{O}$ to Na_2S were kept at 0.5) was slowly added to the above solution and then stirred for 0.5 h. Finally, the product was collected by centrifugation and washed with deionized water and ethanol three times each and vacuum-dried overnight to obtain the final powder (The mole ratios of added Zn^{2+} :CdS NRs were 0, 0.1, 0.5, 1.0, 1.5, 5.0, and the corresponding samples were labeled as CdS/ZnS-0, CdS/ZnS-0.1, CdS/ZnS-0.5, CdS/ZnS-1.0, CdS/ZnS-1.5, and CdS/ZnS-5.0, respectively). Pure ZnS powder sample was prepared following the same procedure without adding CdS NRs. The loading of 1.0 wt% Pt cocatalyst was performed according to a previous report.⁶¹

Characterization. The crystal structures of the samples were investigated by powder X-ray diffraction (XRD, D/max-TTR III) using graphite monochromatized Cu K α radiation of 1.54178 Å, operating at 40 kV and 200 mA. The scanning rate was 10°

min^{-1} from 10° to 70° (2θ). Scanning electron microscopy (SEM) was performed on JSM-6700F. Transmission electron microscopy (TEM) images, high resolution transmission electron microscopy (HR-TEM) images, and mapping images were collected on a JEM-2010 electron microscope, operated at an acceleration voltage of 200 kV. The UV-vis diffuse reflectance spectra was obtained using a UV-visible spectrophotometer (SOLID 3700 UV-vis spectrometer). X-ray photoelectron spectroscopy (XPS) measurement was performed using an ESCALAB 250 X-ray photoelectron spectrometer.

Photocurrent measurement. Photocurrent experiments were measured using a CHI 602E instrument in a standard three-electrode system with the photocatalyst-coated FTO as the working electrode (an active area of $\sim 1 \text{ cm}^2$). An Ag/AgCl was used as a reference electrode and Pt wire as the counter electrode. A 300W Xe lamp with a cut-off filter ($\lambda > 420 \text{ nm}$) was used as the light source, and the electrolyte was sodium sulfate (Na_2SO_4 , 0.5 M) solution. The working electrodes were prepared by dropping a suspension (20 μL) made of CdS, CdS/ZnS-0.5 (the concentration of samples being 50 mg/mL) onto the surface of a precleaned FTO plate using a pipette, then the working electrodes were dried in air at room temperature before the measurements. The applied potential for the measurement was 0.5 V vs Ag/AgCl (saturated KCl).

Photocatalytic hydrogen production. Photocatalytic H_2 production experiments were carried out in a 50 mL round-bottom flask at ambient temperature and atmospheric pressure. A 300 W Xe-lamp equipped with a 420 nm cut-off filter was

used to provide the visible light irradiation. In a typical photocatalytic reaction, 1.0 mg of the powder sample was dispersed in a 20 mL aqueous solution. Before irradiation, the solution was bubbled with high purity nitrogen for 15 min to remove the air inside. Methane was used in the reactor as the internal standard.²⁶ The amount of evolved H₂ was determined with a gas chromatograph (GC) equipped with a TCD detector. The apparent quantum yield (AQY) was measured using a 300 W Xe-lamp equipped with a 420 nm (±5 nm) bandpass cut filter. The AQY was calculated based on the following equation (1):

$$\begin{aligned} \text{AQY}(\%) &= \frac{\text{number of reacted electrons}}{\text{number of incident photons}} \times 100\% \\ &= \frac{\text{number of evolved H}_2 \text{ molecules} \times 2}{\text{number of incident photons}} \times 100\% \end{aligned}$$

Acknowledgements

This work was financially supported by the National Natural Science Foundation of China (21271166, 21473170), the Fundamental Research Funds for the Central Universities, the Program for New Century Excellent Talents in University (NCET), and the Thousand Young Talents Program.

Supporting Information.

Additional characterization data and figures: TEM image, HRTEM image, SEM image and XRD pattern of the photocatalyst after photocatalysis, and the Movie for H₂ production. This information is available free of charge via the Internet at <http://pubs.rsc.org>.

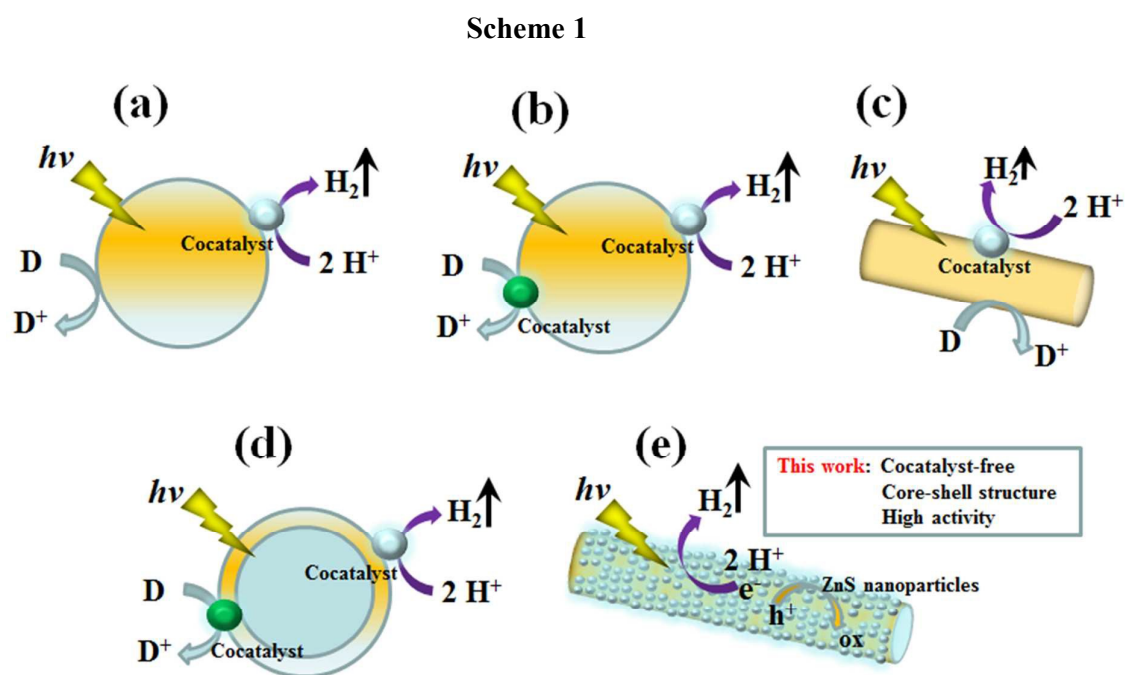
References

- (1) Kudo, A.; Miseki, Y. *Chem. Soc. Rev.* **2009**, *38*, 253-278.
- (2) Zou, Z.; Ye, J.; Sayama, K.; Arakawa, H. *Nature* **2001**, *414*, 625-627.
- (3) Esswein, A. J.; Nocera, D. G. *Chem. Rev.* **2007**, *107*, 4022-4047.
- (4) Concepcion, J. J.; Jurss, J. W.; Brennaman, M. K.; Hoertz, P. G.; Patrocínio, A. O. v. T.; Iha, N. Y. M.; Templeton, J. L.; Meyer, T. J. *Acc. Chem. Res.* **2009**, *42*, 1954-1965.
- (5) Alstrum-Acevedo, J. H.; Brennaman, M. K.; Meyer, T. J. *Inorg. Chem.* **2005**, *44*, 6802-6827.
- (6) Eckenhoff, W. T.; McNamara, W. R.; Du, P.; Eisenberg, R. *Biochim. Biophys. Acta, Bioenerg.* **2013**, *1827*, 958-973.
- (7) Du, P.; Eisenberg, R. *Energy Environ. Sci.* **2012**, *5*, 6012-6021.
- (8) Li, Y. H.; Xing, J.; Chen, Z. J.; Li, Z.; Tian, F.; Zheng, L. R.; Wang, H. F.; Hu, P.; Zhao, H. J.; Yang, H. G. *Nat. Commun.* **2013**, *4*, 2500. doi: 2510.1038/ncomms3500.
- (9) Lu, Y. C.; Lin, Y. H.; Xie, T. F.; Chen, L. P.; Yi, S. S.; Wang, D. J. *ACS Appl. Mater. Interfaces* **2013**, *5*, 4017-4020.
- (10) Zhuang, S. D.; Xu, X. Y.; Feng, B.; Hu, J. G.; Pang, Y. R.; Zhou, G.; Tong, L.; Zhou, Y. X. *ACS Appl. Mater. Interfaces* **2014**, *6*, 613-621.
- (11) Liao, L. B.; Zhang, Q. H.; Su, Z. H.; Zhao, Z. Z.; Wang, Y. N.; Li, Y.; Lu, X. X.; Wei, D. G.; Feng, G. Y.; Yu, Q. K.; Cai, X. J.; Zhao, J. M.; Ren, Z. F.; Fang, H.; Robles-Hernandez, F.; Baldelli, S.; Bao, J. M. *Nat. Nanotech.* **2014**, *9*, 69-73.
- (12) Wender, H.; Goncalves, R. V.; Dias, C. S. B.; Zapata, M. J. M.; Zagonel, L. F.; Mendonca, E. C.; Teixeira, S. R.; Garcia, F. *Nanoscale* **2013**, *5*, 9310-9316.
- (13) Zhang, S. S.; Wang, H. J.; Yeung, M. S.; Fang, Y. P.; Yu, H.; Peng, F. *Int. J. Hydrogen Energy* **2013**, *38*, 7241-7245.
- (14) Maeda, K.; Higashi, M.; Siritanaratkul, B.; Abe, R.; Domen, K. *J. Am. Chem. Soc.* **2011**, *133*, 12334-12337.
- (15) Maeda, K.; Teramura, K.; Lu, D.; Takata, T.; Saito, N.; Inoue, Y.; Domen, K. *Nature* **2006**, *440*, 295.
- (16) Hou, J. G.; Wang, Z.; Kan, W. B.; Jiao, S. Q.; Zhu, H. M.; Kumar, R. V. *J. Mater. Chem.* **2012**, *22*, 7291-7299.
- (17) Matsukawa, M.; Ishikawa, R.; Hisatomi, T.; Moriya, Y.; Shibata, N.; Kubota, J.; Ikuhara, Y.; Domen, K. *Nano. Lett.* **2014**, *14*, 1038-1041.
- (18) Ye, L.; Fu, J. L.; Xu, Z.; Yuan, R. S.; Li, Z. H. *ACS Appl. Mater. Interfaces* **2014**, *6*, 3483-3490.
- (19) Fang, J.; Xu, L.; Zhang, Z. Y.; Yuan, Y. P.; Cao, S. W.; Wang, Z.; Yin, L. S.; Liao, Y. S.; Xue, C. *ACS Appl. Mater. Interfaces* **2013**, *5*, 8088-8092.
- (20) Hong, J. D.; Wang, Y. S.; Wang, Y. B.; Zhang, W.; Xu, R. *Chemsuschem* **2013**, *6*, 2263-2268.
- (21) Wang, X. C.; Maeda, K.; Thomas, A.; Takanabe, K.; Xin, G.; Carlsson, J. M.; Domen, K.; Antonietti, M. *Nat. Mater.* **2009**, *8*, 76-80.
- (22) Chen, X.; Shen, S.; Guo, L.; Mao, S. S. *Chem. Rev.* **2010**, *110*, 6503-6570.
- (23) Li, J.; Yang, J. H.; Wen, F. Y.; Li, C. *Chem. Commun.* **2011**, *47*, 7080-7082.

- (24) Zhong, M.; Shi, J. Y.; Xiong, F. Q.; Zhang, W. H.; Li, C. *Sol. Energy* **2012**, *86*, 756-763.
- (25) Yan, H.; Yang, J.; Ma, G.; Wu, G.; Zong, X.; Lei, Z.; Shi, J.; Li, C. *J. Catal.* **2009**, *266*, 165-168.
- (26) Yan, Z.; Yu, X.; Han, A.; Xu, P.; Du, P. *J. Phys. Chem. C* **2014**, *118*, 22896-22903.
- (27) Yan, Z.; Yu, X.; Zhang, Y.; Jia, H.; Sun, Z.; Du, P. *Appl. Catal., B* **2014**, *160*, 173-178.
- (28) Wen, F.; Li, C. *Acc. Chem. Res.* **2013**, *46*, 2355-2364.
- (29) Sreethawong, T.; Yoshikawa, S. *Catal. Commun.* **2005**, *6*, 661-668.
- (30) Navarro, R.; Del Valle, F.; Fierro, J. *Int. J. Hydrogen Energy* **2008**, *33*, 4265-4273.
- (31) Huang, L.; Wang, X.; Yang, J.; Liu, G.; Han, J.; Li, C. *J. Phys. Chem. C* **2013**, *117*, 11584-11591.
- (32) Lv, X.-J.; Zhou, S.-X.; Zhang, C.; Chang, H.-X.; Chen, Y.; Fu, W.-F. *J. Mater. Chem.* **2012**, *22*, 18542-18549.
- (33) Jang, J. S.; Joshi, U. A.; Lee, J. S. *J. Phys. Chem. C* **2007**, *111*, 13280-13287.
- (34) Yuan, J.; Wen, J.; Gao, Q.; Chen, S.; Li, J.; Li, X.; Fang, Y. *Dalton Trans.* **2015**, *44*, 1680-1689.
- (35) Zhang, J.; Qiao, S. Z.; Qi, L.; Yu, J. *Phys. Chem. Chem. Phys.* **2013**, *15*, 12088-12094.
- (36) Kim, H. N.; Kim, T. W.; Kim, I. Y.; Hwang, S. J. *Adv. Funct. Mater.* **2011**, *21*, 3111-3118.
- (37) Liu, N.; Schneider, C.; Freitag, D.; Hartmann, M.; Venkatesan, U.; Müller, J.; Spiecker, E.; Schmuki, P. *Nano. Lett.* **2014**, *14*, 3309-3313.
- (38) Hu, Z. F.; Yu, J. C. *J. Mater. Chem. A* **2013**, *1*, 12221-12228.
- (39) Cheng, W. Y.; Yu, T. H.; Chao, K. J.; Lu, S. Y. *Int. J. Hydrogen Energy* **2013**, *38*, 9665-9672.
- (40) Wang, X. W.; Liu, G.; Wang, L. Z.; Chen, Z. G.; Lu, G. Q.; Cheng, H. M. *Adv. Energy. Mater.* **2012**, *2*, 42-46.
- (41) Barpuzary, D.; Khan, Z.; Vinothkumar, N.; De, M.; Qureshi, M. *J. Phys. Chem. C* **2012**, *116*, 150-156.
- (42) Xiao, L.; Chen, H.; Huang, J. *Mater. Res. Bull.* **2015**, *64*, 370-374.
- (43) Xie, Y. P.; Yu, Z. B.; Liu, G.; Ma, X. L.; Cheng, H. M. *Energy Environ. Sci.* **2014**, *7*, 1895-1901.
- (44) Wang, J.; Lim, Y.-F.; Ho, G. W. *Nanoscale* **2014**, *6*, 9673-9680.
- (45) Tarafder, K.; Surendranath, Y.; Olshansky, J. H.; Alivisatos, A. P.; Wang, L.-W. *J. Am. Chem. Soc.* **2014**, *136*, 5121-5131.
- (46) Zhu, H.; Song, N.; Lian, T. *J. Am. Chem. Soc.* **2013**, *135*, 11461-11464.
- (47) Deka, S.; Quarta, A.; Lupo, M. G.; Falqui, A.; Boninelli, S.; Giannini, C.; Morello, G.; Giorgi, M. D.; Lanzani, G.; Spinella, C.; Cingolani, R.; Pellegrino, T.; Manna, L. *J. Am. Chem. Soc.* **2009**, *131*, 2948-2958.
- (48) Nelson, J. *Phys. Rev. B* **1999**, *59*, 15374-15380.
- (49) van de Lagemaat, J.; Frank, A. J. *J. Phys. Chem. B* **2001**, *105*, 11194-11205.
- (50) Tang, J.; Huo, Z.; Britzman, S.; Gao, H.; Yang, P. *Nat. Nanotech.* **2011**, *6*, 568-572.
- (51) Wu, K.; Zhu, H.; Lian, T. *Acc. Chem. Rec.* **2015**, *48*, 851-859.
- (52) Wang, H.; Chen, Z.; Cheng, Q.; Yuan, L. *J. Alloys Compd.* **2009**, *478*, 872-875.
- (53) Xu, J.; Ji, W. *J. Mater. Sci. Lett.* **1999**, *18*, 115-117.
- (54) Sang, H. X.; Wang, X. T.; Fan, C. C.; Wang, F. *Int. J. Hydrogen Energy* **2012**, *37*,

- 1348-1355.
- (55) Zhu, B.; Lin, B.; Zhou, Y.; Sun, P.; Yao, Q.; Chen, Y.; Gao, B. *J. Mater. Chem. A* **2014**, *2*, 3819-3827.
- (56) Zhang, J.; Wang, L.; Liu, X.; Li, X. a.; Huang, W. *J. Mater. Chem. A* **2015**, *3*, 535-541.
- (57) Raubach, C. W.; Santana, Y. V. B. d.; Ferrer, M. M.; Longo, V. M.; Varela, J. A.; Avansi Jr., W.; Buzolin, P. G. C.; Sambrano, J. R.; Longo, E. *Chem. Phys. Lett.* **2012**, *536*, 96-99.
- (58) Zhang, J.; Wang, Y.; Zhang, J.; Lin, Z.; Huang, F.; Yu, J. *ACS Appl. Mater. Interfaces* **2013**, *5*, 1031-1037.
- (59) Thibert, A.; Frame, F. A.; Busby, E.; Holmes, M. A.; Osterloh, F. E.; Larsen, D. S. *J. Phys. Chem. Lett.* **2011**, *2*, 2688-2694.
- (60) Datta, A.; Panda, S. K.; Chaudhuri, S. *J. Phys. Chem. C* **2007**, *111*, 17260-17264.
- (61) Wang, Y.; Wang, Y.; Xu, R. *J. Phys. Chem. C* **2013**, *117*, 783-790.

Figures:



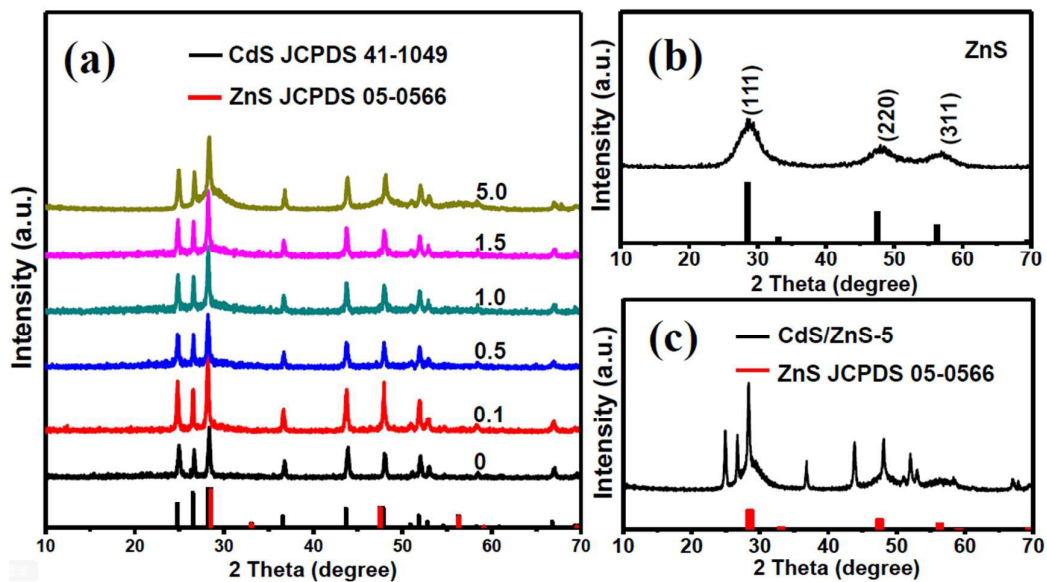


Figure 1. (a) Powder XRD patterns of CdS/ZnS NRs photocatalysts with different ratios of Zn²⁺. (b) Powder XRD patterns of pure ZnS. (c) Powder XRD patterns of CdS/ZnS-5 sample.

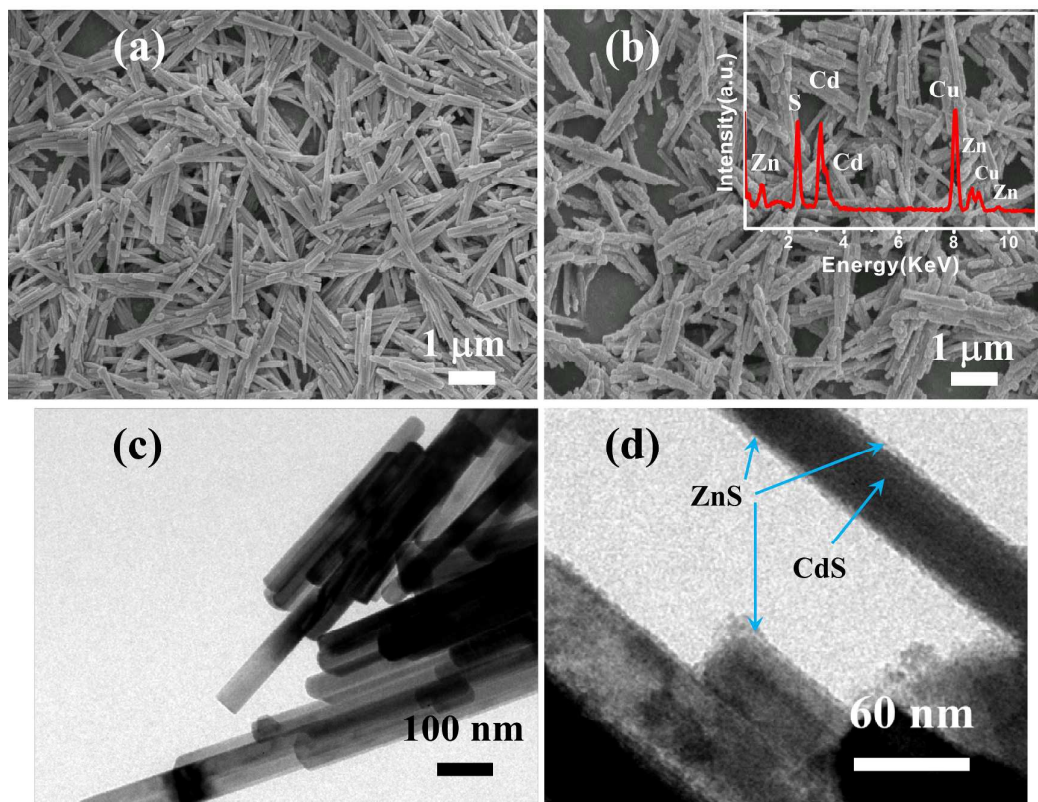


Figure 2. (a) SEM image of pure CdS NRs. (b) SEM image of CdS/ZnS-0.5 NRs photocatalyst. (c) TEM image of pure CdS NRs. (d) TEM image of CdS/ZnS-0.5 NRs photocatalyst.

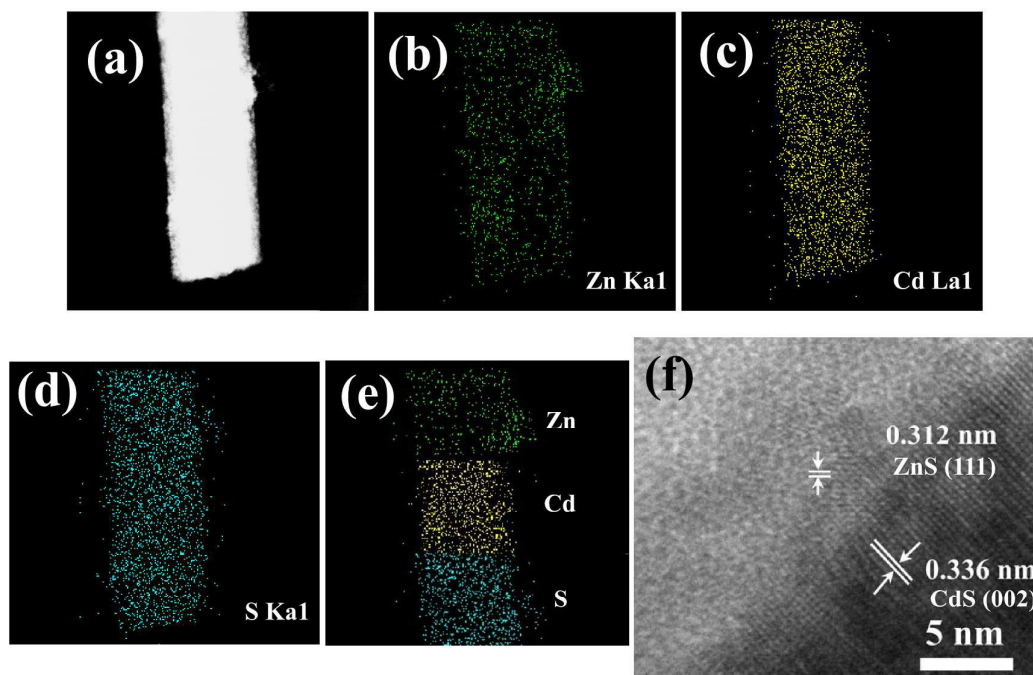


Figure 3. (a) Bright field image of CdS/ZnS-0.5 photocatalyst. (b-d) EDX mapping of the elemental distribution of CdS/ZnS-0.5 photocatalyst. (e) Difference in distribution of Zn, Cd, and S elements. (f) HRTEM image of CdS/ZnS-0.5 photocatalyst.

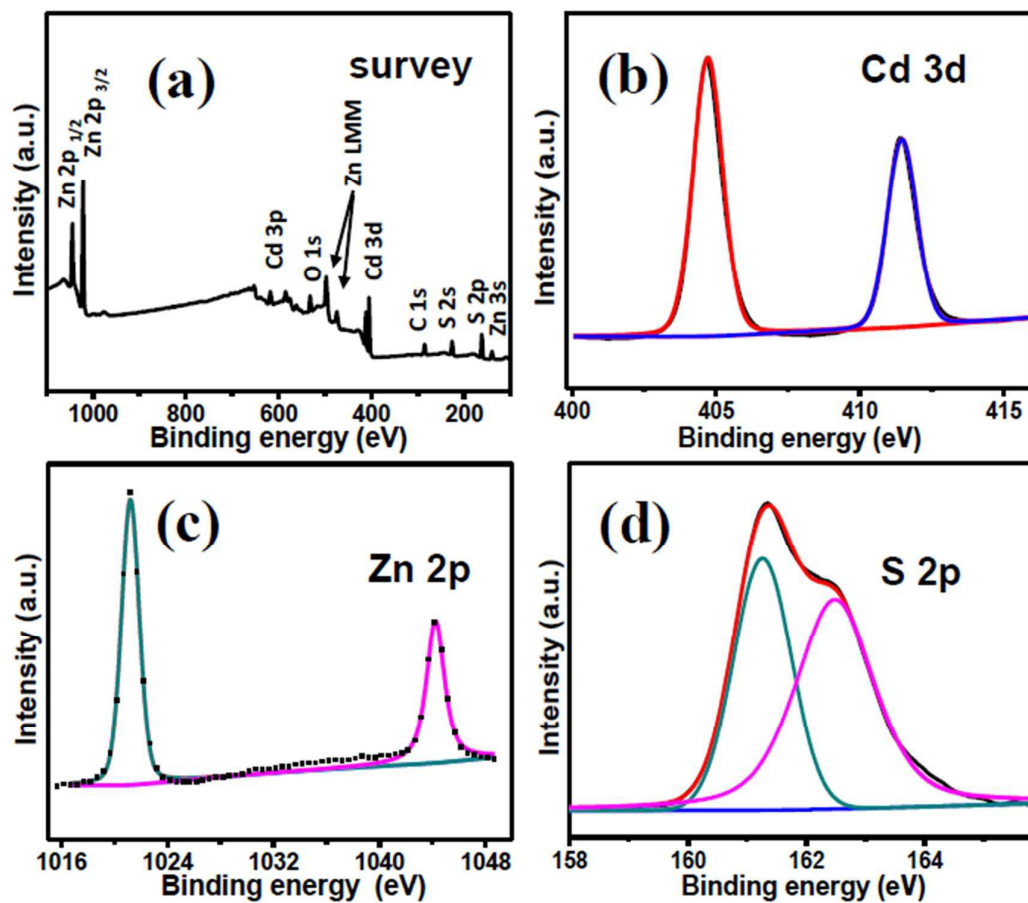


Figure 4. (a) XPS survey spectrum of CdS/ZnS-0.5 sample. High-resolution XPS spectra of (b) Cd 3d; (c) Zn 2p; (d) S 2p.

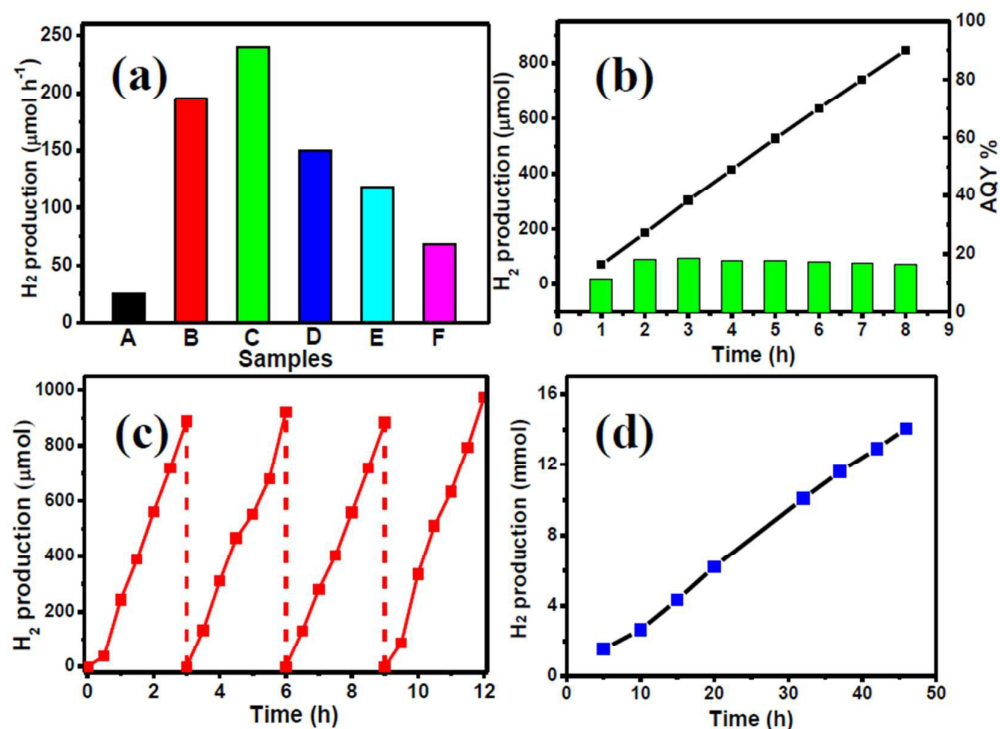


Figure 5. (a) Hydrogen evolution rate in a 20 mL aqueous solution containing 0.75 M Na₂S and 1.05 M Na₂SO₃ in the presence of 1.0 mg of CdS/ZnS NRs photocatalysts. A: CdS/ZnS-0, B: CdS/ZnS-0.1, C: CdS/ZnS-0.5, D: CdS/ZnS-1.0, E: CdS/ZnS-1.5, F: CdS/ZnS-5.0. (b) The time courses of H₂ production and apparent quantum yield (AQY) over CdS/ZnS-0.5 NRs photocatalyst under monochromatic 420 nm light irradiation using 1.0 mg photocatalyst in a 20 mL aqueous solution containing 0.75 M Na₂S and 1.05 M Na₂SO₃. The bars represent the apparent quantum yields. (c) Cyclic H₂ evolution curves for 1.0 mg CdS/ZnS-0.5 NRs photocatalyst in a 20 mL aqueous solution containing 1.125 M Na₂S and 1.575 M Na₂SO₃. (d) Long-term photocatalytic H₂ production over CdS/ZnS-0.5 NRs photocatalyst for 46 hours under visible light irradiation at ambient temperature. The system contained 1.0 mg photocatalyst, 1.25 M Na₂S, and 1.75 M Na₂SO₃ in 50 mL deionized water. Generally, the light source was a Xe lamp (300 W) with a 420 nm cut-off filter.

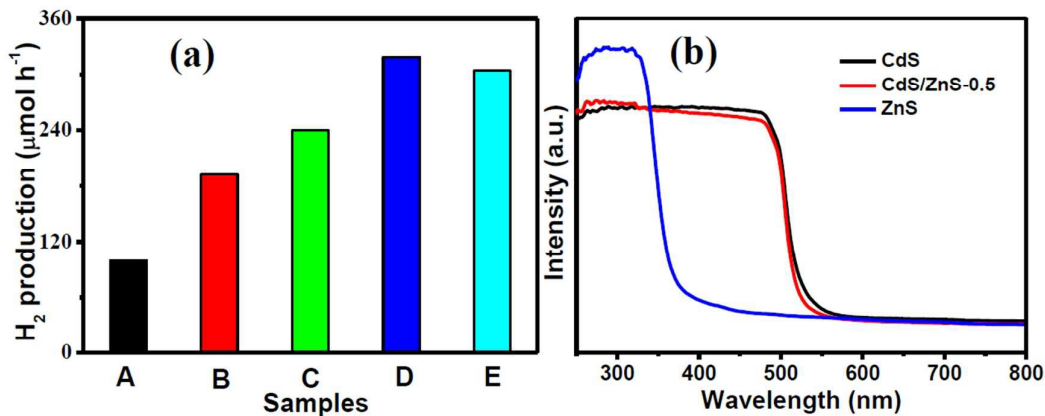


Figure 6. (a) The rate of H₂ production using CdS/ZnS-0.5 NRs photocatalyst under different concentrations of electron donors at ambient temperature under visible light ($\lambda > 420$ nm): (A) 0.25 M Na₂S, 0.35 M Na₂SO₃; (B) 0.50 M Na₂S, 0.70 M Na₂SO₃; (C) 0.75 M Na₂S, 1.05 M Na₂SO₃; (D) 1.0 M Na₂S, 1.4 M Na₂SO₃; (E) 1.25 M Na₂S, 1.75 M Na₂SO₃. (b) UV-vis diffuse reflectance spectra of the CdS, CdS/ZnS-0.5, and ZnS samples.

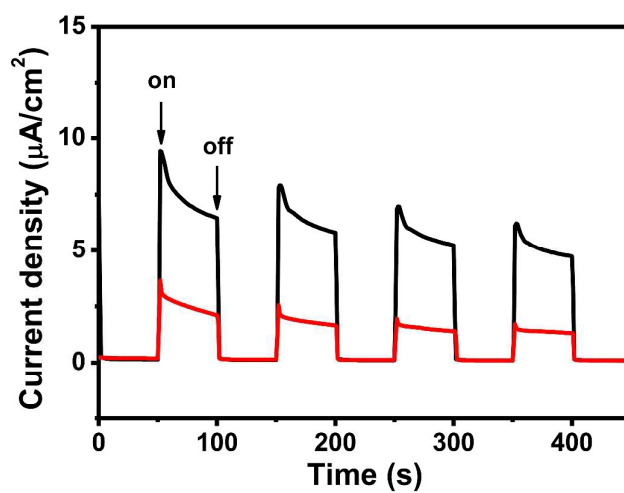
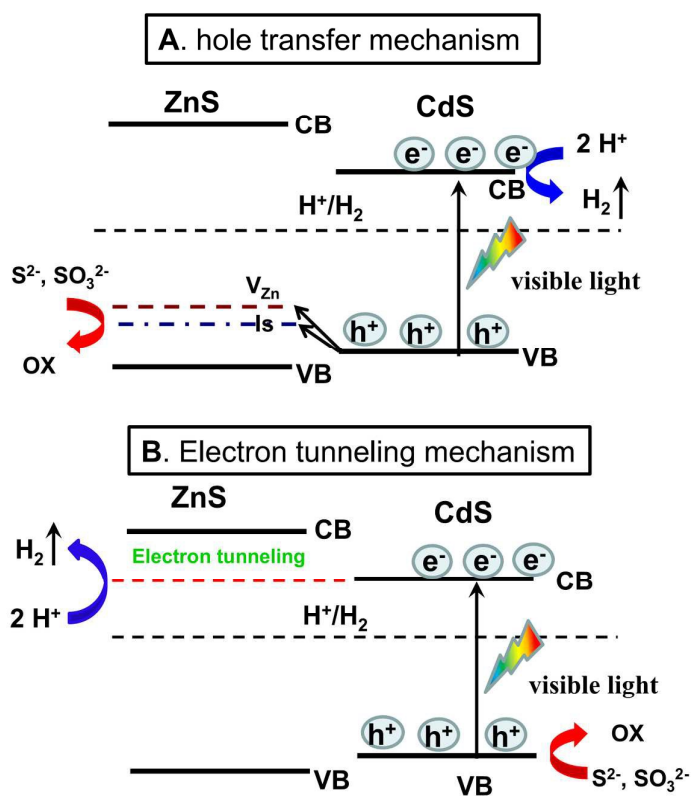


Figure 7. Photocurrent density of CdS and CdS/ZnS-0.5 samples measured at 0.5 V vs. Ag/AgCl under chopped (on-off) 300 W Xe lamp ($\lambda > 420$ nm) in a 0.5 M Na_2SO_4 aqueous solution.



Scheme 2. Schematic illustration of the mechanisms for the photocatalytic H_2 production over core/shell CdS/ZnS NRs under visible light irradiation.

Table of contents

